In *Turbulence and Magnetic Fields in Astrophysics*. Edited by E. Falgarone and T. Passot.
Lecture Notes in Physics, Vol 614. Springer, 2003. ISBN 3-540-00274-X.

Coronal Heating and Reduced MHD

Sean Oughton[1], Pablo Dmitruk[2], and William H. Matthaeus[2]

[1] Department of Mathematics, University of Waikato, Hamilton, New Zealand
[2] Bartol Research Institute, University of Delaware, Newark, DE 19716, USA

Abstract. We review the use of reduced magnetohydrodynamics (RMHD) in coronal heating models, with particular emphasis on models for magnetically open regions. A brief review of the nature of the coronal heating problem is presented first, followed by detailed discussion regarding the assumptions and features of RMHD and its applicability to the dynamics of the solar corona. We then review a class of heating models based on quasi-2D turbulent cascades driven by low-frequency Alfvén waves.

1 Introduction

The fact that the solar corona is over a hundred times hotter than the visible solar surface was first established in 1939 [1,2]. Observations indicate that coronal temperatures are typically $\sim 10^6\,\mathrm{K}$, while the temperature of the photosphere is $\approx 6000\,\mathrm{K}$. Although much effort has been expended in attempts to explain this "coronal heating problem", the mechanism underlying the heating process is still not known; see, e.g., [3–7]. In this paper we review first the role of reduced magnetohydrodynamics (RMHD) in coronal dynamics and second a class of heating models which employ RMHD processes in a central way.

Note that it is the *mechanism* of coronal heating which has remained unidentified, not the energy source for the heating. An ample reservoir of energy is available to heat the corona, in the form of the (convectively) turbulent photospheric and subphotospheric motions. The associated energy flux is essentially equivalent to the Poynting flux $\boldsymbol{S} = \boldsymbol{E} \times \boldsymbol{B}$, where the electric field is that induced by the convective motions [8]. Thus, the "problem" in the coronal heating problem is primarily concerned with how to transport this energy up into the corona and then convert it into heat within a few solar radii ($R_{\mathrm{sun}} = 700\,\mathrm{Mm}$). Recent observations [9–13] emphasize that the bulk of the heating needs to occur within this distance, which is a rather strong constraint.

Table 1 lists some of the heating models which have been proposed over the last 60 years. Although no one heating theory has been entirely successful, substantial progress in understanding the situation has nonetheless occurred. A key recognition is that the corona is magnetically dominated, in the sense that there is a large (often approximately vertical) mean magnetic field ($\boldsymbol{B}_0$) throughout it, with the fluctuations in the velocity and magnetic fields being much smaller in magnitude [6,14,15]. As discussed in the subsequent sections, this physical situation of a strong $\boldsymbol{B}_0$ with small (but finite) amplitude fluctuations can be exploited to simplify the full 3D MHD equations to those of reduced MHD. Figure 1 is a sketch depicting the magnetic structure of the corona.

Table 1. Some candidate heating mechanisms for the solar corona (after Ulmschneider 1996 [5]; see also [4])

Energy Carrier	Dissipation Mechanism
Acoustic waves Slow mode MHD waves Longitudinal MHD waves	Shocks
Fast mode MHD waves	Landau damping
Magnetoacoustic surface waves	Phase mixing Mode coupling Resonant absorption
Alfvén waves	Mode coupling Phase mixing Resonance heating Viscous heating Turbulent heating Landau damping
Current sheets	Reconnection (turbulent/wave heating)
Magnetic field	Nanoflares

Most of the approaches listed in Table 1 can be characterized as *direct*, in the sense that the energy of the energy carrier is converted directly into heat without passing through any other channel. On the whole, direct methods have so far proved to be either insufficient or inadequate (e.g., [4]), thereby prompting consideration of indirect methods. In an *indirect* heating method the free energy source in the corona is first converted into some other form of excitation, which is itself subsequently converted into heat energy.

Various other divisions of the heating models have been employed, for example wave versus turbulence and acoustic versus magnetic. In the latter case, the magnetic mechanisms are often subdivided into either AC (aka wave) mechanisms, wherein the field guides the (dissipative) waves, and DC (aka current) mechanisms where it is the dissipation of the energy stored in the magnetic field which provides the heating [3,4,8,16,17]. In this review we pay particular attention to an indirect turbulence heating model, where the (quasi-2D) turbulence is driven by low-frequency Alfvén waves.

Note that the traditional schism between wave models and turbulence models can be misleading and/or over-restrictive. A similarly misleading schism has also featured in models for the transport and evolution of solar wind fluctuations [18–21]. However, in both the corona and the solar wind, observations indicate that the systems are strongly dynamic with wave and turbulence processes each

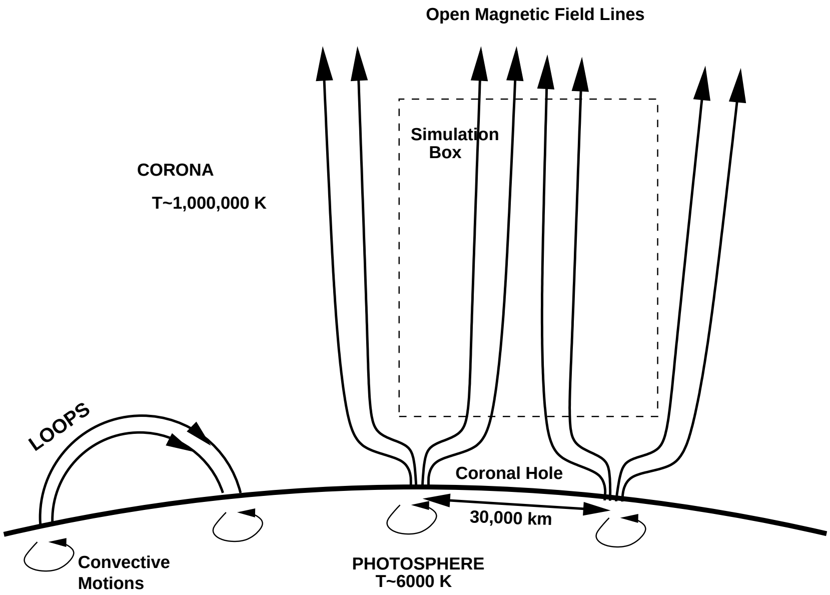

Fig. 1. Cartoon sketch of the (magnetic) structure of the corona. Shown are a few magnetic field-lines delineating coronal loops and coronal holes. Also indicated are the convective motions which power the atmospheric heating. Plasma heating in both the magnetically open and the magnetically closed regions remains unexplained. Note that at photospheric heights the magnetic flux bundles are typically spatially well separated. In contrast, the coronal field is essentially space filling, with adjacent flux bundles subject to shear due to the independent motion of the photospheric "footpoints"

playing important roles, and, moreover, that activity occurs over a wide range of spatial and temporal scales amenable to MHD-based descriptions. For example, in the corona measurements from various satellite and ground-based instruments show the presence of waves and substantial transverse (to the local vertical) structuring (see, e.g., [7,22]). Observations of counter-propagating waves [11] and reconnection [23] have also been reported, although in such cases a unique interpretation of the data is often not possible. Taken together, the observations imply that coronal dynamics involves both wave effects and nonlinear MHD effects, such as turbulent reconnection and cascades.

The remainder of the paper is organised as follows. Section 2 contains a detailed discussion of the assumptions and characteristics of reduced MHD, along with a critique of their relevance to the corona. In Section 3 we review several coronal heating models which employ RMHD, focusing primarily on models for magnetically open regions. The final section summarises our conclusions. Two appendices, one a brief history of RMHD derivations and the other on the subtle relationship between RMHD fluctuations and solutions of the RMHD equations, close the paper.

2 Reduced MHD

The equations of reduced MHD, first derived by Strauss [24], can be obtained by considering the strong $\boldsymbol{B}_0$, low-frequency limit of the full 3D MHD equations. Note that they are *not a linearization* of the MHD equations—the nonlinear terms are always important, by construction. The RMHD equations have also been derived from various other perspectives, some of which are summarised in Appendix A.

In this section, we begin by stating the RMHD equations and then derive the timescale condition which determines whether or not a fluctuation is RMHD in character. Subsection 2.2 is a discussion of the nature of cascades in RMHD turbulence and their relation to cascades in full 3D turbulence. Subsection 2.3 reviews the relevance of RMHD to coronal dynamics.

2.1 Equations and Timescale Conditions

The usual primary assumption of RMHD is that there is a strong uniform magnetic field, $\boldsymbol{B}_0 = B_0\hat{\boldsymbol{z}}$, present [24–26]. The field is strong in the sense that the amplitudes of the velocity and magnetic field fluctuations are small. Since the full 3D MHD equations have terms like $\boldsymbol{B}_0 \cdot \nabla \boldsymbol{b}$, these terms will be much larger than the nonlinear ones (e.g., $\boldsymbol{v} \cdot \nabla \boldsymbol{v}$), unless gradients along $\boldsymbol{B}_0$ are restricted to be small, as is the case for RMHD. When this situation is enforced, the natural coordinates to use involve a rescaling of the parallel (z) coordinate to be purely large-scale and of B_0 to be O(1).

The RMHD equations are then conveniently written—using non-dimensionalized (Alfvén speed) units—as equations for the evolution of the fluctuations in the fluid vorticity $\omega(x, y, z, t)$ and the magnetic vector potential $a(x, y, z, t)$:

$$\left(\frac{\partial}{\partial t} + \boldsymbol{v}\cdot\nabla_\perp\right)\omega = \boldsymbol{b}\cdot\nabla_\perp j + \nu\nabla_\perp^2\omega + B_0\frac{\partial j}{\partial z}, \tag{1a}$$

$$\left(\frac{\partial}{\partial t} + \boldsymbol{v}\cdot\nabla_\perp\right)a = \eta\nabla_\perp^2 a + B_0\frac{\partial \psi}{\partial z}, \tag{1b}$$

where $\nabla_\perp = (\partial_x, \partial_y, 0)$, $\boldsymbol{v} = \nabla \times \psi\hat{\boldsymbol{z}}$, $\boldsymbol{b} = \nabla \times a\hat{\boldsymbol{z}}$, $\omega = -\nabla_\perp^2\psi$, $j = -\nabla_\perp^2 a$, $\nabla_\perp \cdot \boldsymbol{v} = 0$, and the other symbols have their usual meanings (see, e.g., [25]). Since the equations are written using Alfvén speed units, B_0 is actually the (large-scale) Alfvén speed. However, it is often convenient to still refer to it as the mean field. We emphasize that the z coordinate has been rescaled such that only large-scale variations with z are permissible. For example, the final term in (1a) can be rewritten as

$$\left(\frac{B_0}{\epsilon}\right)\left(\epsilon\frac{\partial}{\partial z}\right)j, \tag{2}$$

where a small parameter ϵ appears explicitly (see below). The two terms in brackets then correspond directly to the actual physical mean field and the gradient operator along it [25].

It is evident that in RMHD the velocity is incompressible and that setting $B_0 = 0$ would yield precisely the equations of incompressible 2D MHD, on a set of independent z-planes. On the other hand, if the only terms retained are the time derivatives and the terms involving B_0, the solutions are parallel-propagating (transverse) Alfvén waves. Thus it is clear that the B_0 terms provide the explicit coupling between the otherwise independent planes of 2D excitation.

A related point is that while $\boldsymbol{v}$ and $\boldsymbol{b}$ depend upon all three spatial coordinates (although as noted the z dependence is "slow") the amplitudes of these excitations are confined to the planes perpendicular to $\boldsymbol{B}_0$.[1] In this sense, the RMHD equations are complementary to systems employing $2\frac{1}{2}$D geometry, wherein vector fields have three components but depend on only two spatial coordinates.

A derivation of the equations is now sketched. Consider a fluctuating magnetofluid[2] threaded by a uniform magnetic field $\boldsymbol{B}_0$. The dynamics of the fluctuations is given by the usual 3D MHD equations in the presence of a mean field. In order to compare the characteristic timescales associated with these fluctuations, it is useful to employ a Fourier decomposition. Accordingly the mean square magnetic fluctuation $\langle b^2 \rangle$ may be decomposed into a spectral distribution. The magnetic energy spectrum, i.e., the distribution of energy over wavenumber magnitude k, may be designated as $E_b(k)$, and satisfies

$$\frac{\langle b^2 \rangle}{2} = \int_0^\infty E_b(k)\,\mathrm{d}k. \tag{3}$$

The contribution to the magnetic energy density due to fluctuations near spatial scale $1/k$ may be estimated in the usual way as $b_k^2 = kE_b(k)$.

In incompressible MHD each Fourier mode has two[3] timescales associated with it:

$$\tau_{\mathrm{A}}(\boldsymbol{k}) = \frac{1}{|\boldsymbol{k} \cdot \boldsymbol{B}_0|} \equiv \frac{1}{|k_\parallel||\boldsymbol{B}_0|}\ , \tag{4a}$$

$$\tau_{\mathrm{NL}}(\boldsymbol{k}) = \frac{1}{kb_k}\ , \tag{4b}$$

where these are respectively referred to as the Alfvén (or wave) timescale and the (direction-averaged) modal nonlinear timescale; $k_\parallel$ is the component of the Fourier wavevector parallel to $\boldsymbol{B}_0$. Two points regarding the Alfvén timescale are noteworthy. First, it is the time it takes an Alfvén wave to propagate a parallel wavelength for the mode (modulo a factor of 2π), and is thus quite distinct from the box-crossing timescale of a wave, which for a box of length L_{box} would be $\tau_{\mathrm{box}} = L_{\mathrm{box}}/B_0$, independent of $\boldsymbol{k}$. Second, it depends strongly on the orientation of its wavevector but is *in*dependent of the energy of the fluctuation.

---

[1] This is not quite the full story. For a derivation beginning from the incompressible equations [25], it can be shown that, to the same order as (1a) and (1b), RMHD also involves fluctuations whose amplitudes are purely parallel to $\boldsymbol{B}_0$. For a derivation beginning with compressible MHD [26] the parallel fluctuations are down by a factor equal to the turbulent Mach number (interestingly, this relative ordering of the parallel amplitude also emerges in incompressible and compressible simulations of the *full* MHD equations [27]). However, in both cases these parallel fluctuations are dynamically passive and thus of reduced interest [25,26].

[2] Density fluctuations are likely to be of interest along with the velocity and magnetic fluctuations.

[3] Where the viscous and resistive timescales are not considered.

The nonlinear timescale as defined in (4b) is local and direction-averaged (over all $\boldsymbol{k}$ with the same $|\boldsymbol{k}|$). Consequently, it cannot be viewed as anything other than a reasonable approximation in the present context, which is expected to be highly anisotropic. Its analogue for hydrodynamic turbulence is, however, familiar and reliable in the context of incompressible homogeneous hydrodynamic turbulence [28], and therefore it is believed that this type of estimate is a good starting point for MHD as well. It is also useful to define the *global* nonlinear timescale $\tau_{\mathrm{NL}} = \lambda_\perp/\delta b$, where $\lambda_\perp$ is a lengthscale characteristic of the turbulent (nonlinear) dynamics[4] and $\delta b = \sqrt{\langle b^2 \rangle}$ is the root mean square magnetic fluctuation (assumed $\approx \delta v$).

Forming the ratio of the *modal* timescales yields the central parameter of RMHD:

$$\epsilon_{\mathrm{RMHD}}(\boldsymbol{k}) = \frac{\tau_{\mathrm{NL}}(\boldsymbol{k})}{\tau_{\mathrm{A}}(\boldsymbol{k})} = \frac{k_\parallel}{k} \frac{B_0}{b_k}. \tag{5}$$

This is the ratio of the timescale associated with wave-like activity, which depends upon parallel structure, to the timescale of nonlinear activity, which does not depend upon direction at the current level of approximation. Physically, it appears likely that the set of (Fourier) modes which satisfy $\tau_{\mathrm{NL}}(\boldsymbol{k}) \lesssim \tau_{\mathrm{A}}(\boldsymbol{k})$—that is those modes for which the wave timescale is *not* dominant—will behave quite differently from those for which it is. Thus, we partition the modes on the basis of the inequality $\epsilon_{\mathrm{RMHD}}(\boldsymbol{k}) \lesssim 1$, and investigate the governing equations for the two sets of modes.[5] As it turns out, the modes which satisfy this inequality are the RMHD ones.

Note that the *critical balance* condition employed by Goldreich and Sridhar [29] in a paper on strong MHD turbulence is essentially the condition $\epsilon_{\mathrm{RMHD}}(\boldsymbol{k}) = 1$, and is thus related to the boundary between RMHD and non-RMHD fluctuations (cf. Appendix B and Fig. 7a).

Up to this point no major assumptions about the nature of the fluctuations, or the geometry of the system, have been made. As noted above, the usual primary assumption of RMHD is that $\boldsymbol{B}_0$ is a strong field, meaning that its energy density is much greater than that of the fluctuations. Consequently, for each Fourier mode $B_0/b_k \gg 1$, and satisfaction of $\epsilon_{\mathrm{RMHD}}(\boldsymbol{k}) \lesssim 1$ requires that $k_\parallel \ll k$. In other words, the RMHD modes have wavevectors which are approximately perpendicular to $\boldsymbol{B}_0$. This leads to two approximations employed frequently in RMHD, namely $k \approx k_\perp$ and $\tau_{\mathrm{NL}}(\boldsymbol{k}) \approx 1/(k_\perp b_k)$.

---

[4] The "$\perp$" subscript is included since we have in mind specialisation to the RMHD case.

[5] For systems which are not in steady-state the partitioning is likely to be time-dependent.

The Strauss [24] and Montgomery [25] derivations of the RMHD equations are perturbation expansions in distinct but related small parameters. Respectively, $\epsilon_{\text{Strauss}} = \ell_\perp / \ell_\parallel$ and $\epsilon_{\text{Mont}} = \delta b / B_0$, where the ℓs are characteristic lengthscales in the directions indicated by their subscripts (relative to $\boldsymbol{B}_0$). Note that these small parameters are based on global, not modal, quantities. RMHD provides the leading-order dynamics for each of these derivations (cf. Appendix A).

Subsequently, Zank and Matthaeus [26] noted that a more rigorous derivation is also possible. They showed that the 3D *compressible* MHD equations have leading-order solutions which obey the RMHD equations, provided that (i) the sonic Mach number, $M_{\text{s}} = \delta v / c_{\text{s}}$, is small, (ii) the plasma beta,[6] β_{p}, is at most of order unity, (iii) characteristic lengths along B_0 are much longer than those perpendicular to it, and (iv) all high-frequency[7] modes have been eliminated. It is condition (iv) which ties their derivation of the RMHD equations to the timescale-based discussion of the RMHD modes presented above.

Note that there is a subtle but important distinction to be made between the set of RMHD *fluctuations* and solutions of the RMHD *equations*. It is quite possible to solve the RMHD equations using initial conditions which include non-RMHD fluctuations, e.g., in simulations with rectangular domains in k-space (see Fig. 7a). The solutions to the equations at later times would, presumably, also include contributions from non-RMHD fluctuations. Several questions then arise as to the consistency of the RMHD equations. For example: Do they adequately capture the physics of non-RMHD fluctuations along with that of the RMHD fluctuations? If an (initial) solution to the RMHD equations contains only RMHD modes, how rapidly will non-RMHD modes be generated? Do RMHD solutions "escape" from the range of validity of the equations themselves? Concerns such as these have prompted some implementations of RMHD to include *ad hoc*—and perhaps unnecessary—parallel dissipation terms which damp energy production at high $k_\parallel$. Further discussion regarding this point is presented in Appendix B.

2.2 Anisotropy and Cascades

The RMHD equations are manifestly anisotropic, containing as they do a strong mean magnetic field with the (dynamically important) fluctuations strictly perpendicular to it. Associated with this is the lengthscale anisotropy between the x and y coordinates and the slowly-varying z coordinate These anisotropies have important consequences for the development and interpretation of RMHD energy cascades.

In RMHD the cascade is such that excitations are principally driven towards high *perpendicular* wavenumbers [25,30,31]. That is, the evolution in physical space involves the development of structure with finer and finer scale perpendicular to $\boldsymbol{B}_0$ (with the smallest scales attained set by the Reynolds numbers).

---

[6] The plasma beta factor, β_{p}, is the usual ratio of thermal and magnetic pressures.

[7] Where high-frequency is defined to be on the acoustic timescale or faster.

This inherent feature of RMHD is often identified by referring to a *strong perpendicular cascade.* It should be kept in mind, however, that it is the parallel cascade which is substantially weakened in RMHD, rather than the perpendicular cascade being strengthened [30–34].

To understand the weakening of the parallel cascade it is helpful to consider cascades in fully 3D (i.e., not reduced) MHD turbulence when $\delta b/B_0$ is small. Considering the turbulent fluctuations as Alfvén wavepackets, the strength of B_0 means that the packets are rapidly propagating. Hence, the (nonlinear) interaction time for two counter-propagating wavepackets is much reduced, leading to a weakened cascade. There is, however, an escape clause, since this argument ignores the anisotropy of the wave dispersion relation $\omega_{\mathrm{A}} = \boldsymbol{k} \cdot \boldsymbol{B}_0$. If one or more of the wavepackets has large spatial extent (i.e., has a characteristic $k_{\|}$ which is small)—as is the case for RMHD fluctuations—then even though they are moving rapidly through each other, the interaction time for the packets can still be long, and in particular of order τ_{NL} rather than $1/(kB_0)$. Consequently the cascade associated with these interactions is only weakly affected by the strong B_0. Shebalin et al. [33] presented a "weak turbulence" analysis of such interactions which revealed that *strict* resonant driving occurs only when a propagating mode interacts with a non-propagating (i.e., 2D) mode of opposite cross helicity (see also [35,36]). In such cases the driven mode has exactly the same $k_{\|}$ as that driving mode which is propagating. Thus, in the weak turbulence limit there is strong perpendicular spectral transfer but *no parallel spectral transfer.* The arguments can be generalised to allow for broadened resonant interactions [30,31], and one finds that the interaction of an arbitrary propagating mode with an RMHD mode also leads to strong perpendicular cascade.

Additional support for suppressed parallel cascade with still strong perpendicular cascade comes from analytic work, and compressible and incompressible simulations with a strong mean field [25,27,30–33,37–42]. Moreover, these studies indicate that turbulence which is initially isotropic dynamically reorganises to favor RMHD-type fluctuations. For example, one can examine the evolution of mean wavenumbers computed parallel and perpendicular to B_0 using simulations. Figure 2, reproduced from [31], displays results from two (unforced) incompressible 3D MHD simulations with different values of B_0. When $B_0 = 0$, the mean $k_\perp$ and $k_{\|}$ are essentially the same at all times, showing a monotonic increase as the nonlinear interactions cause transfer of energy to smaller scales, followed by a gradual decline as the turbulence decays. Such isotropy is of course expected when there is no preferred direction. For the $B_0 = 4$ case, in contrast, the mean $k_{\|}$ remains almost constant, indicating that the cascade in this direction has been strongly suppressed. The mean $k_\perp$, however, behaves in the same way as it did in the $B_0 = 0$ simulation.[8]

There is a technical point about the full-MHD perpendicular cascade that warrants mention at this point, namely that it consists of two distinct parts

---

[8] The maximum value attained, however, is somewhat less than in the isotropic case since the initial conditions contain both RMHD and non-RMHD fluctuations and the latter are influenced by B_0 while the anisotropy is developing.

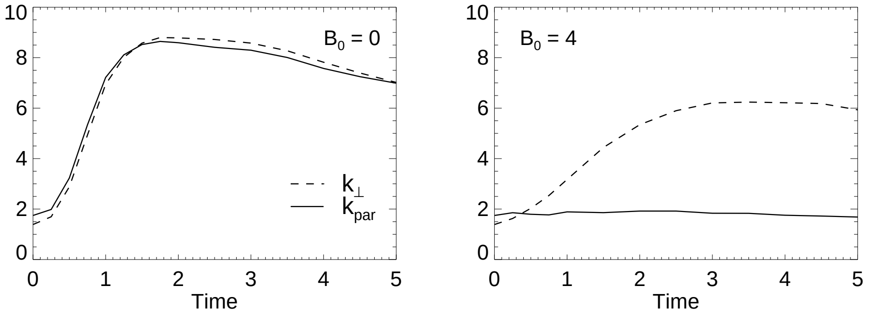

Fig. 2. Mean parallel and perpendicular wavenumbers as a function of time for two fully 3D MHD simulations. The simulations are unforced and have the same initial conditions and Reynolds numbers but different values of B_0. A value of $B_0 = 1$ corresponds to equipartition of the energy in the initial turbulent fluctuations and that in the mean field. Note the lack of evolution in $k_\parallel$ for the $B_0 = 4$ case (figure courtesy of [31])

[30,31]. The first part involves the self-interactions of only the RMHD modes. As these are in effect "zero-frequency" modes, the interactions are (trivially) always resonant. Perpendicular cascade proceeds unimpeded for RMHD modes. Moreover, because the resonance condition is trivial, it does not impose any additional restrictions on parallel spectral transfer, provided that excitations remain within the RMHD region $\epsilon_{\mathrm{RMHD}} \lesssim 1$. Thus, RMHD spectral transfer is essentially isotropic although its region of applicability is emphatically not (cf. Fig. 7). The second type of perpendicular cascade in full-MHD comes from modes that are outside the RMHD region. Sufficiently far outside the $\epsilon_{\mathrm{RMHD}} = 1$ boundary the resonance conditions described by Shebalin et al. [33,35,38,42,43] prevail, and the only surviving incompressible couplings are those that maintain constant $k_\parallel$. This resonant cascade of high-frequency modes to higher $k_\perp$ is nonlocal, since it relies upon driving by (inherently) low-frequency RMHD modes.

2.3 Relevance in the Corona

Here we briefly summarise some of the theoretical and observational support for using RMHD in studies of coronal dynamics.

As noted above, an important characteristic of both coronal holes and coronal loops is that they are permeated by a strong large-scale magnetic field. Moreover, the large-scale field can be approximated as uniform over significant distances (e.g., fractions of a loop length).

Observations of coronal quantities [11,44–46] in magnetically open regions suggest that $\delta v \approx 25$–$35\,\mathrm{km\,s^{-1}}$, $c_{\mathrm{s}} \approx 115\,\mathrm{km\,s^{-1}}$, and that Alfvén speeds are in excess of $1000\,\mathrm{km\,s^{-1}}$. Thus, $M_{\mathrm{s}} = \delta v / c_{\mathrm{s}} \approx 0.2$–$0.3$ and $\beta_{\mathrm{p}} \approx 0.01$, consistent with the assumptions underlying RMHD derivations.

The timescales of the processes involved in heating models can also be examined for consistency with the assumptions of RMHD. In estimating a coronal value for $\tau_{\mathrm{NL}} = \lambda_\perp / \delta v$ we may take $\lambda_\perp$ to be in the range 3–30 Mm, where the upper value is given by the size of super-granules (equivalent to the magnetic network separation distance). This yields $\tau_{\mathrm{NL}} \approx 10^2$–$10^3$ s. Now let us consider, somewhat arbitrarily, the parallel system size to be one solar radius.[9] Using a nominal Alfvén speed of $1000\,\mathrm{km\,s^{-1}}$, the associated τ_{box} is 700 s. The longest period waves that fit within the system thus have $\epsilon_{\mathrm{RMHD}} \approx 1$. Hence, for RMHD to be sensibly applied, the driving fluctuations should have periods which are of order a few hundred seconds or longer. Fluctuations associated with $\tau_{\mathrm{A}} > \tau_{\mathrm{box}}$ do not "fit" within the system, and the nomenclature "low-frequency waves" gives way to "quasi-static fluctuations" as this inequality becomes progressively better satisfied. However, both low-frequency waves and quasi-static fluctuations can be dynamically included in the RMHD formulation.

Continual buffeting from the granular and super-granular motions associated with the convective dynamics of the interior is believed to be the source of the driving fluctuations and can excite Alfvén waves which propagate upwards along the (mean) field in magnetically open regions.[10] Observations indicate that the timescale associated with the coronal base driving fluctuations is $\tau_{\mathrm{ph}} \sim 10^3$–$10^4$ s [7,8,47], which is clearly much longer than the estimates for τ_{NL}.

For magnetically closed regions, like coronal loops, both ends of the "coronal box" are anchored in the photosphere, where the granular motions induce continual displacements of the field-lines. Provided again that those motions proceed on a slow scale, compared to the typical nonlinear time, the RMHD condition will be satisfied. (See the end of Sect. 3.2 for an important distinction between the wave box-crossing time and the modal Alfvénic time in connection with consideration of the RMHD condition.)

In summary, there are good theoretical and observational grounds for using RMHD to study the dynamics of coronal plasma. Parcels of the corona typically have: low β_{p}, a strong approximately uniform magnetic field with low fluctuation levels ($\delta b/B_0 \ll 1$), and $\epsilon_{\mathrm{RMHD}} \lesssim 1$, all of which are in accord with the assumptions underlying RMHD. Thus, we expect that RMHD-based models will capture the essential physics of the low-frequency waves, quasi-static fluctuations, and turbulence that we wish to investigate. From a practical perspective, RMHD also affords considerable advantages in numerical simplicity and efficiency. Naturally, results from RMHD models will only provide an approximation to the true dynamics since, among other effects, it is highly likely that compressibility and kinetic processes will play important roles.

---

[9] This choice is not entirely without justification since observations indicate that heating in open field-line regions operates within about a solar radius above the photosphere.

[10] Similarly, buffeting and other processes (e.g., reconnection events) in the chromosphere and transition region may also excite Alfvén waves or related propagating fluctuations. For the heating model(s) considered below the actual source of the fluctuations is not particularly important. What is important is that such fluctuations are present at some (perhaps only notional) coronal base.

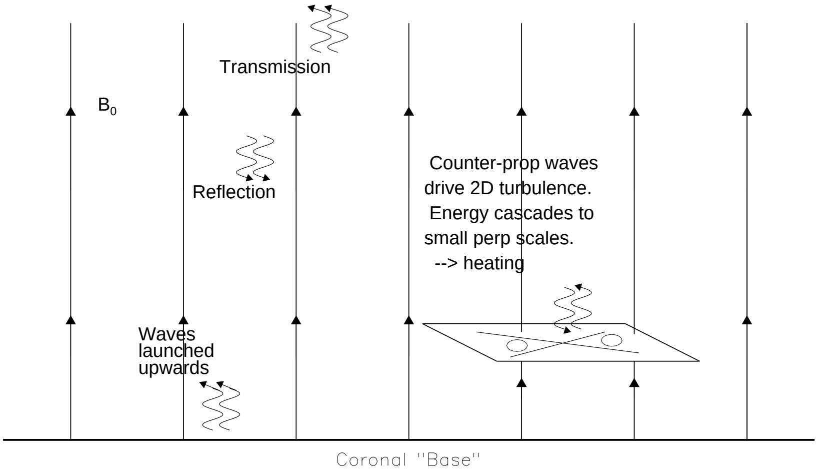

Fig. 3. Cartoon sketch of the heating model for magnetically open regions. Low-frequency waves are reflected off inhomogeneities in the large-scale density and magnetic field. The ensuing population of counter-propagating modes interacts to drive an RMHD (quasi-perpendicular) turbulent cascade, with the energy at the small-scale end of the cascade being converted into heat by kinetic processes

3 Coronal Heating Models

3.1 Coronal Holes

The class of models to be described was first presented by Matthaeus et al. [48] and has subsequently been investigated using phenomenology based models and nonlinear simulations [49–53]. As we shall see, an important distinguishing factor between the various models is the degree of realism and self-consistency associated with the reflection and driving terms.

Figure 3 is a schematic representation of the physics associated with the proposed heating scenario. *Low*-frequency Alfvénic fluctuations, generated somewhere below the coronal base, propagate up into the corona. Whilst progressing through the corona they undergo (*non*-WKB) reflection off the gradients in the background density and magnetic fields. This produces a population of counter-propagating fluctuations, which interact. The interaction is nonlinear and, because the modes are low-frequency, predominantly acts to drive *quasi-2D* fluctuations; these then self-interact to produce a cascade of energy towards small *perpendicular* lengthscales, with the formation of current sheets and the reconnection of transverse magnetic islands featuring prominently in the dynamics. Kinetic effects at these scales convert the turbulent energy into heat.

Models of this kind exhibit several features [51] which void some of the criticisms which have been leveled at direct wave heating models. For example, the usual criticism of (direct) wave heating models in magnetically open regions is that, because of the large propagation speeds ($\sim 10^3\,\mathrm{km\,s^{-1}}$), Alfvén waves propagate out of the region where the heating needs to occur (within $\approx 2\,R_{\mathrm{sun}}$

of the surface) before they can be significantly damped [54,55]. However, in the above indirect model, the waves lose energy primarily due to (nonlinear) transfer of excitation to the quasi-2D turbulent cascade, rather than (direct) viscous and resistive wave damping. For the low-frequency waves considered in the model, this is a relatively fast process and associated with the extraction of significant amounts of wave energy. Provided there is a region containing a population of low-frequency counter-propagating waves these will interact nonlinearly to drive a sustained quasi-2D cascade. Naturally, the *strength* of the cascade will depend on factors such as the abundance of upward and downward propagating modes (and hence the reflection rate), and the wave amplitudes, but the cascade's *existence* is not unduly constrained by the large Alfvén speed.

Note that direct wave damping models usually rely on damping of high-frequency (e.g., ion cyclotron) waves, whereas the class of models described above extracts energy from low-frequency waves. There are several advantages to using low-frequency waves as the input energy source. First, photospheric observations indicate that there is substantial energy in this range of the frequency power spectrum, whereas the spectrum at high frequencies ($\sim$ kHz), although unobserved, is expected to be of much lower amplitude [55–57]. Second, non-WKB reflection due to inhomogeneities in the solar atmosphere is most efficient for low-frequency fluctuations [58–61].

Another feature of the model depicted in Figure 3 is that since the cascade is quasi-2D, both its dynamics and the associated heat output at small perpendicular scales are largely insensitive to the strength of B_0 [27,33,34,37,38].[11] This aspect may be of relevance in explaining why coronal heating appears to depend only weakly on solar cycle phase. Moreover, since the nascent solar wind is relatively sluggish over the height range where the counter-propagating fluctuations interact [12], one concludes that the heating occurs "in place." This follows since when the low-frequency waves supply energy to the cascade at a height r_1, say, the quasi-2D cascade transfers the energy to small scales at about this same height. Thus, a quasi-2D cascade, coupled with low wind speed, helps circumvent problems associated with the rapid removal of energy from the desired heating region by fast propagating waves.

We turn now to several studies of specific models within the above class of heating model. Note that at least two points make the RMHD equations a natural choice for use in investigating such models. First, the driving in the model is via low-frequency (and hence long wavelength) Alfvén waves propagating along a strong $\boldsymbol{B}_0$. Second, the primary couplings of such counter-propagating waves are to (Fourier) modes with wavevectors which are quasi-perpendicular to $\boldsymbol{B}_0$.

---

[11] Although the existence of a sufficiently strong B_0 may well be required in order to produce a substantial population of quasi-2D fluctuations in the first place. Moreover, even though the existence and strength of a quasi-2D cascade may be insensitive to the strength of B_0, the wave transmission out of the system and reflection within the system may retain a dependence upon B_0. Thus, the relative strength of turbulence versus wave effects at a fixed frequency of driving is expected to remain sensitive to the size of the Alfvén speed. It is only for the idealized case of "zero-frequency driving" that complete insensitivity to B_0 would be expected.

The initial investigation was via a one-point homogeneous turbulence closure for the energy in the upwards (Z_+^2) and downwards (Z_-^2) quasi-2D/RMHD fluctuations. Terms representing the forcing (F), energy-conserving reflection ($R^\pm$), and transmission (T) (see Fig. 3) were included using *ad hoc* rates [49],

$$\frac{dZ_-^2}{dt} = -\frac{Z_-^2 Z_+}{\lambda_\perp} + F - R^- Z_-^2 + R^+ Z_+^2 - T Z_-^2, \tag{6a}$$

$$\frac{dZ_+^2}{dt} = -\frac{Z_+^2 Z_-}{\lambda_\perp} + R^- Z_-^2 - R^+ Z_+^2. \tag{6b}$$

The model was closed by including an equation for the evolution of the characteristic transverse lengthscale of the quasi-2D fluctuations, $\lambda_\perp$, giving a (numerically) tractable system of three nonlinear ODEs [49].

In such a one-point closure the simulation "box" (Fig. 1) shrinks to a point and only volume-averaged information is available. Despite this simplicity, the model has proved to be remarkably robust, giving heating efficiencies in excellent agreement with models where the nonlinearities are treated with considerably more sophistication. In particular, in the limit that the reflection rate is much greater than the transmission rate, one can show analytically that the dissipation rate approaches $F/2$ asymptotically (from below). Defining the *heating efficiency* as the dissipation rate divided by the rate of energy injection, one finds that the maximum heating efficiency is 50% (see Fig. 5).

More sophisticated investigations of the heating scenario can be achieved using spectral method simulations of the nonlinear dynamics [51,53]. Such an approach is superior to the turbulence phenomenology in the sense that it does not assume that the turbulence is self-sustaining, allowing for the possibility that the heating mechanism may not be viable. When performing such simulations, the basic equations of RMHD, (1a,b), require augmenting with terms which account for the forcing, reflection, and transmission. In the simplest case [51] this is achieved using terms which are essentially the same as their analogs in the phenomenology, i.e., F is a body force, and $R^\pm$ and T are imposed rates.

Figure 4 shows time histories of several interesting quantities from a (periodic) RMHD simulation of this kind [51], with Reynolds numbers of 800, $F = 1$, $R = R^\pm = 0.5$, and $T = 0.3$. The initial conditions involve a seed level of turbulence, with the excited fluctuations having their perpendicular wavenumbers restricted to the band $2 \leq k_\perp \leq 6$ and an approximately flat spectrum in $k_\parallel$. It is evident that a statistically steady state is reached after a few tens of box crossing times. These states are characterised by mixed (normalised) cross helicity[12] $\sigma_c = \langle \boldsymbol{v} \cdot \boldsymbol{b} \rangle / (\langle \boldsymbol{v}^2 \rangle + \langle \boldsymbol{b}^2 \rangle)$, with around 10% of the energy contained in the *strictly* non-propagating (i.e., 2D) fluctuations. Note that the mean-square current is, visually, a much more intermittent quantity than the energy. Examination of the probability density functions of these quantities confirms this impression, with strongly non-gaussian tails characterising the current fluctuations [51]. Since in

---

[12] As well as being the average correlation between $\boldsymbol{v}$ and $\boldsymbol{b}$, cross helicity is also interpretable as the difference between the energy in upward and downward type fluctuations, e.g., [35,62,63]. Angle brackets denote spatial averaging.

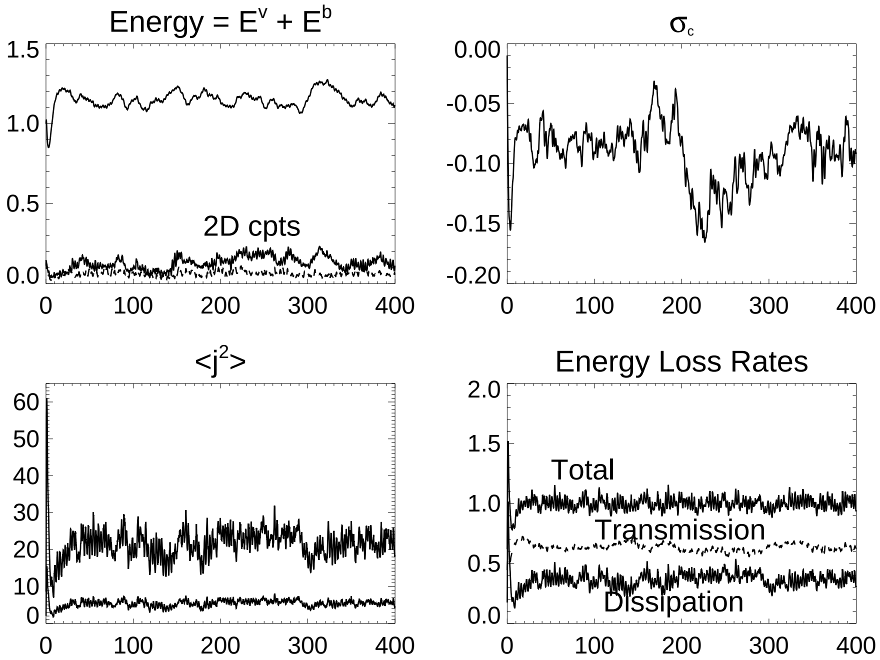

Fig. 4. Time histories from a $256^2 \times 4$ periodic RMHD simulation of the heating model discussed in the text. Shown are the energy, normalised cross helicity (which is bounded by ± 1), mean-square current, and energy loss rates. In the lefthand panels, the lower traces are the contributions to the totals due to the 2D (non-propagating) components. The unit of time is a box-crossing time for an Alfvén wave (after [51])

this incompressible model the heating is due to viscous and resistive dissipation, it is no surprise that the dissipation is also quite intermittent [64,65].

Examination of energy spectra and transverse cross sections in coordinate space (not shown; see [51]) emphasizes that the dynamics is turbulent with broadband spectra, transient current sheets, and reconnection events clearly evident. It is also shown that the long-time statistical properties of the system are insensitive to the total energy of the initial fluctuations, indicating that the heating process is robust.

A central question which all coronal heating models must address concerns their efficiency. Given an input source of energy, how much of it can be sustainably converted into heat within a few solar radii? In the case of the phenomenology and the simulations, it is straightforward to calculate the steady-state rates of dissipation and transmission. Figure 5 plots these two quantities (normalised to the energy injection rate) for a range of reflection rates. The data points are from the RMHD simulations [51] while the curves are calculated using the phenomenology solutions [49]. Remarkably, the results from the simple one-point phenomenology are in excellent accord with those from the full simulations. A key feature which the plot reveals is that even when the reflection rate is very

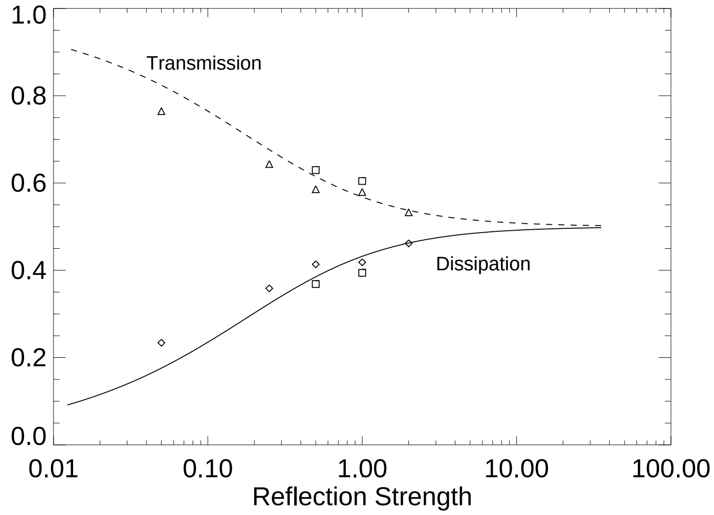

Fig. 5. Rates of dissipation and transmission for the one-point phenomenology (*curves*) and forced periodic RMHD simulations with resolutions of $256^2 \times 4$ (*squares*) and $64^2 \times 4$ (*other symbols*), respectively corresponding to Reynolds numbers of 800 and 200. Quantities are normalised to the energy injection rate, so that the dissipation rate is equivalent to the heating efficiency. Note the excellent agreement between the (simulation) data points and the solutions to the phenomenology, even when the reflection rate is small

weak (e.g., ~ 0.01), the models still yield heating efficiencies of $\sim 10\%$. Note that if the reflection is switched off in either model, the dissipation in the unforced modes decays to zero, so that sustained turbulent heating is not achieved [51,52]. This point is elaborated on shortly.

In summary, results obtained from the phenomenology and the periodic simulations indicate that heating efficiencies of 10%–50% are easily attainable—provided that *some* reflection of the upward propagating low-frequency fluctuations takes place. Given even rather small reflection rates, counter-propagating waves will drive—and sustain—a quasi-2D cascade for a wide range of initial conditions [51].

While these results are encouraging it is evident that they are only a first step. Some of the limitations concern the periodic nature of the boundary conditions and that forcing, reflection, and transmission are included in an *ad hoc* fashion. Models which include these effects in a more self-consistent way are clearly needed.

Recently, Dmitruk et al. [52] have extended the above models by including modeled (mean) coronal density and magnetic field profiles, with the reflection and transmission calculated from these in a consistent manner. Moreover, their heating model also better addresses both the transport of the fluctuations and the driving at the lower boundary. The basic physics is a more realistic implementation of the scenario sketched in Figure 3, with upward propagating fluctuations injected at the base, initial conditions involving a seed level of broadband (RMHD) turbulence, and (height dependent) reflection coefficients proportional to the derivative of the large-scale Alfvén velocity. A key feature is that the boundary conditions are no longer periodic.

Using this model Dmitruk et al. investigated the following question: *Under what circumstances can one sustain incompressible (R)MHD turbulence in open geometries when it is driven using unidirectionally propagating Alfvén waves?*[13] In these circumstances it is convenient to use the Elsässer potentials as the basic variables, rather than the vorticity/vector potential formulation employed in (1a,b). Specifically, one introduces the potential for the upwards-type fluctuations, $f = \psi - a$, and that for the downwards-type ones, $g = \psi + a$. We use the word "type" to indicate that not all the fluctuations are propagating, since in general the averages of f and g over the parallel coordinate (denoted s rather than z in [52]) are non-zero. These averages correspond precisely to the existence of non-propagating "structures,"[14] which we refer to as 2D modes, e.g., $\boldsymbol{v}_{2\mathrm{D}}$ where $\partial_s \boldsymbol{v}_{2\mathrm{D}} = 0$.

To address the above question, Dmitruk et al. employed a simulation domain which is periodic in the transverse directions but bounded in the parallel direction by the planes $s = 0$ and $s = 1$. The equations solved are a modification of the basic RMHD equations which allow for a mean field which depends on s, and thus they include reflection in a self-consistent way [61,66,67]. This would introduce a term $\sim j\,\mathrm{d}B_0/\mathrm{d}z$ in (1a), for example. The numerical algorithm employs Fourier-Fourier-Chebyshev spectral collocation with second-order Runge–Kutta timestepping.

Two types of "open" boundary condition were employed on the end s-planes. They correspond to setting either $f = F_0(x, y, t)$ on $s = 0$ and $g = 0$ on $s = 1$, or to setting $\partial_s f = \hat{F}_0(x, y, t)$ on $s = 0$ and $\partial_s g = 0$ on $s = 1$ (i.e., Dirichlet versus Neumann boundary conditions). Since waves are permitted to propagate freely out of the box, there is no need to control the "other" potential on the top and bottom planes as it corresponds to the outward propagating characteristic there. In both cases, the flux of downward waves at the top boundary is enforced to be zero. Physically, one may think of the two types of boundary condition as allowing or disallowing the presence of non-propagating 2D fluctuations [52].

This leads to four fundamentally distinct situations to investigate, made up of the combinations of the two types of boundary condition paired with the presence or absence of reflection (which depends on whether B_0 is a function of s or uniform). Dmitruk et al. examined these situations by driving the $s = 0$ boundary with an F_0 or $\hat{F}_0$ which was monochromatic, meaning that it was sinusoidal in time, with fixed frequency ν, and that only a single transverse

---

[13] It is well known that in incompressible MHD there are *no* nonlinear interactions when *only* unidirectionally propagating fluctuations are present, i.e., either $\boldsymbol{v} = \boldsymbol{b}$ everywhere, or $\boldsymbol{v} = -\boldsymbol{b}$ everywhere.

[14] Note that these structures are not assumed to be static or even steady. In general they should be treated as 2D or $2\frac{1}{2}$D turbulence.

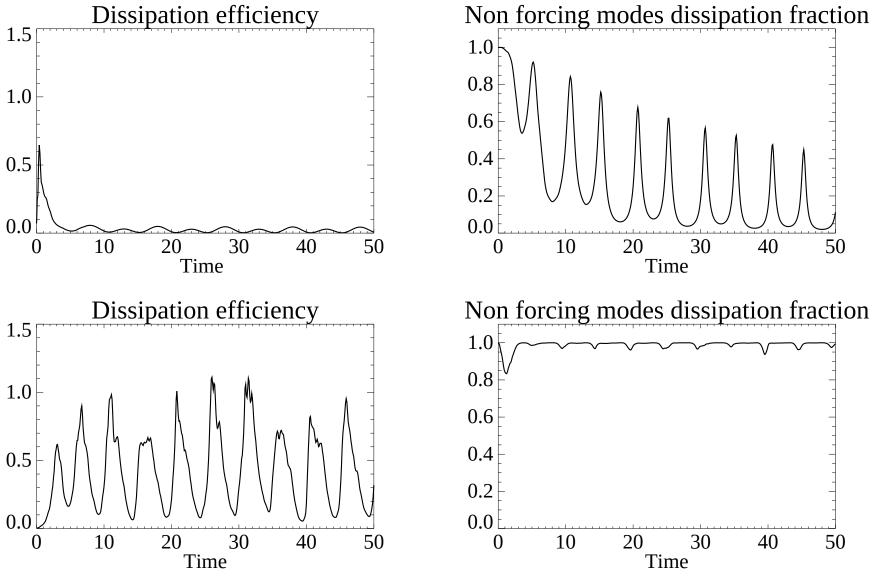

Fig. 6. Heating efficiencies for two runs with boundary conditions which support the presence in the system of non-propagating structures. **Left**: ratio of the dissipation rate to the (period-averaged) input wave energy flux. **Right**: fraction of the dissipation rate which is due to the undriven modes. **Top row**: no reflection. **Bottom row**: reflection. Note that the unit of time is τ_{box}

wavevector (Fourier mode) was so driven. In order to make connection with the coronal context, they employed low-frequency driving with $\nu = 0.1/\tau_{\text{box}}$. Detailed discussion and explanation of the results is given in their paper [52]. Below we summarise their main result.

Figure 6 displays the heating efficiencies, as a function of time, for two runs from [52]. The plots on the top row are for the case where the boundary conditions support structures but there is no reflection (i.e., $\partial_s g = 0$, B_0 uniform). Since there is then no mechanism for generating downwards fluctuations, the cross helicity eventually becomes unidirectional. This can be interpreted as the turbulence being turned off due to *dynamic alignment*[15] [62,63]. Thus, although there is significant turbulent dissipation for tens of τ_{box}, this is not sustained over longer timescales. By contrast, the structures-plus-reflection situation (bottom row) does yield sustained turbulent heating, and, moreover, does so with considerable efficiency.

In the other two cases (not shown; see [52]), where there are no structures present, the turbulent dissipation is negligible after a few τ_{box}. In the absence of reflection this occurs because although the initial conditions contained both upwards and downwards propagating fluctuations, the downwards ones propagate out through the lower boundary in one box-crossing time, leaving only unidirectionally propagating modes. On the other hand, when reflection is active it facilitates the production of additional downward propagating modes. However, these only interact with the propagating upwards modes (since no 2D modes are present), and the interaction time is too short to allow a significant level of turbulence to be maintained.

---

[15] Maron and Goldreich [68] have recently rechristened dynamic alignment as “growth of imbalance”.

Thus, it is only in the "reflection plus structures" cases that sustained turbulent heating ensues. Examination of the energy spectra for these cases verifies that the turbulence is broadband, with the suggestion of a (short) inertial range. As in the periodic RMHD simulations, intense transient current sheets are again evident [52].

It is well known that (incompressible) MHD turbulence, and hence turbulent heating, cannot be sustained solely by unidirectionally propagating waves, e.g., [62,69–72]. The conclusion from the above studies is that two conditions must be satisfied if turbulence in magnetically open regions is to be sustained. These are that (i) there exists some source of downward fluctuations, such as reflection, and (ii) low-frequency "non"-propagating fluctuations, sometimes referred to as structures or quasi-2D turbulence are present. In other words, in the open boundary situation, reflection is no longer the only crucial parameter. It is also necessary to have boundary conditions which support the sustained existence of non-propagating modes.

3.2 Coronal Loops

RMHD-based models for the heating of magnetically closed regions have been in use rather longer than those for open regions, e.g., [73–89,8,47,65]. Mandrini et al. [90] have given a recent review of loop heating models in general, and Gomez et al. [91] have reviewed models which employ MHD turbulence. Here we note a few points regarding heating in loops and the RMHD approximation. We make no attempt to be comprehensive in our treatment, referring the interested reader to the above reviews for further details.

The common basic idea—often referred to as the Parker model [73]—is that the very high electrical conductivity of the photospheric and coronal plasma allows photospheric motions to drive magnetic stresses in the corona,[16] twisting the field-lines and generating transverse components to the velocity and magnetic field fluctuations. As mentioned in the introduction, the fundamental question is how the energy in these large stresses is transferred to smaller scales, where it can be efficiently dissipated. MHD turbulence is a naturally appealing mechanism for achieving such nonlinear energy transfer [91]. Comparisons of the scaling of the heating laws for loop heating models with coronal observations [90], suggest that models involving the gradual stressing of the magnetic field are generally in better agreement with the observations than those involving driving by high-frequency fluctuations (aka “wave heating” models), although the latter are not ruled out.

---

[16] The "frozen field" approximation.

The point we wish to stress here is the similitude between heating models for magnetically closed (loops) and magnetically open (holes) regions when the motions driving the heating are slow. This similarity exists despite the differences between the boundary conditions and the order of magnitude of the involved length and timescales. In effect, a coronal loop driven (at both ends) by low-frequency photospheric motions can be thought of as an open coronal region, where partial or total reflection[17] is imposed at both the upper and lower boundaries. This “end reflection” provides the population of counter-propagating fluctuations needed for sustainment of incompressible MHD turbulence. Features like perpendicular small-scale structures (current sheets), transverse Kolmogorov-like spectra, and intermittent dissipation are strikingly similar in both closed [91] and “open plus reflection” [51] coronal simulations, confirming the analogy.

In closing this subsection we note that some coronal loop heating studies (e.g., [8,64]), state the RMHD (global) timescale condition as $\tau_{\mathrm{NL}} > \tau_{\mathrm{A}}$, which superficially appears to contradict the the condition stated in Sect. 2.1. This apparent problem is actually a consequence of different definitions of τ_{A}. In the context of coronal loops, τ_{A} is often defined to be the time it takes an Alfvén wave to traverse the loop lengthwise. Herein, however, this timescale is denoted by τ_{box}, since it is independent of the wave’s $\boldsymbol{k}$. The statement that the crossing time for the loop (τ_{box}) is less than the timescale based on the (perpendicular) structure of the fluctuations (τ_{NL}) is closely connected with the nature of the motions perturbing the system. The slow motions of the photospheric plasma induce quasi-static low-frequency perturbations in the loop plasma. It is essentially a matter of definition that such low-frequency motions are associated with waves that “do not fit” within the box, since in an unbounded medium they would have wavevectors $\boldsymbol{k}_{\mathrm{ph}}$ which satisfy $k_{\mathrm{ph}} L_{\mathrm{box}} \ll 1$. Nonetheless, one finds (see [64,89]) that $\tau_{\mathrm{NL}}(\boldsymbol{k}_{\mathrm{ph}}) \sim \tau_{\mathrm{box}}$, so that the RMHD condition $\epsilon_{\mathrm{RMHD}}(\boldsymbol{k}_{\mathrm{ph}}) < 1$ is still marginally satisfied even for the shortest wavelength (quasi-static) Alfvén modes, for which $\tau_{\mathrm{A}}(\boldsymbol{k}) = \tau_{\mathrm{box}}$.

4 Conclusions

In this brief review we have attempted to show why reduced magnetohydrodynamics (RMHD) models can be made relevant to applications in coronal heating. In particular, RMHD can capture the physics of propagation, reflection, and cascade of incompressible MHD fluctuations in models of the lower solar atmosphere. The essential reasons behind the viability of RMHD models for the corona are that the Alfvén speed is large, the plasma beta (thermal pressure/magnetic pressure) is small, and the characteristic lengthscales across the large-scale magnetic field are quite likely much smaller than those along it. In addition, there is expected to be a plentiful supply [14] of energy to drive the quasi-2D turbulence, in the form of low-frequency Alfvén waves (generated in the photosphere and/or the chromosphere).

---

[17] The degree of reflection depends on the nature and strength of the photospheric velocity field.

Two clear conclusions have emerged from RMHD studies of low-frequency-driven turbulent heating in regions of open magnetic field-lines, such as coronal holes. The first is that some mechanism for generating counter-propagating fluctuations from unidirectional ones is essential to these models. This requirement has been investigated using both *ad hoc* parameterizations of reflection, as well as models in which the reflection rates are computed consistently from the Alfvén speed profile that is implied by the model adopted for the background coronal magnetic field and density. In each case the conclusion is that turbulence, cascade, and efficient heating can be maintained given sufficient reflection to sustain a population of inward propagating-type modes. This population, surprisingly, may be adequate at a level of just a few percent of the total turbulence energy budget. The second feature that has emerged clearly in these models is the importance of the non-propagating structures (2D turbulence) to the sustainment of the turbulent cascade. The physical reason for this is plain enough: all modes other than the non-propagating ones drain out of the system in an Alfvén crossing time for the system. For a model to work without quasi-2D structures being present, turbulence must be fully replenished through nonlinear processes in a time shorter than this. This is possible, but difficult. Models in which non-propagating structure is permitted have the advantage that 2D fluctuations (which are highly turbulent) stay "in place", in spite of propagation effects that affect other modes.

An observation that can be made at this point is that the differences between heating models for open field-line corona and coronal loops may not be so great, when the analogy between the role of the reflection and the pairing of photospheric boundaries (footpoint motions) is taken into account. Each ensures that a supply of counter-propagating fluctuations will be maintained. While the lengthscales and other physical parameters in loops and coronal holes can be quite different, it still may be that a similar style of model is relevant in both cases.

One aspect of heating models we have not addressed here is whether a sufficient supply of fluctuations reaches the coronal base, a problem that impacts most if not all coronal heating models. Although we shall not discuss this in any detail, it is worth noting that only a small fraction of the fluctuation energy that is apparently available in the photosphere is needed [92], and that observations suggest that fluctuations with the required 20–30 $\mathrm{km\,s^{-1}}$ amplitudes may be present at the coronal base [11,93].

Another subject that we have not delved into is the issue of kinetic dissipation [34]. In the RMHD cascade models it is very clear that the dissipation occurs in randomly formed and highly dynamic sheets or filaments of electric current density. This gives rise to phenomena associated with highly turbulent reconnection [94], including turbulent dissipation of energy into heat. In a cascade picture the exact details of the mechanism of dissipation are not expected to influence the rate of dissipation itself. However, it is a matter of considerable interest to identify the processes that would absorb the flux of cascaded energy. This is especially true in the corona, which is collisionless, so that the dissipative terms typically employed in turbulence calculations are probably inappropriate, particularly those based on scalar (and uniform) resistivity and viscosity. (They do, however, provide the sink at high wavenumber needed for the turbulence picture to function properly.)

A complete picture of coronal dissipation associated with quasi-2D cascade has not yet been developed. However it seems likely that two recently investigated elements will come into play. Studies of laminar spontaneous reconnection (e.g., [95]) indicate that Hall effects become important and that the reconnection zone takes on a characteristic structure determined by electrons and protons at the scale of the ion gyroradius or at the ion inertial scale. Secondly, the parallel electric fields associated with turbulent reconnection should rapidly produce strong electron beams. In their nonlinear phase these beams form electron "phase space holes" that propagate rapidly along the large-scale magnetic field. (These are observed in the geospace environment in conditions that are analogous to the corona in some interesting ways. See, e.g., [96]). Whether or not the scattering of protons by these high-frequency electron phenomena can give rise to the high perpendicular temperatures observed in the corona by spectrometers such as UVCS [9,10] has yet to be determined. If it can, then this mechanism would provide an alternative to the direct cyclotron damping mechanism often invoked for coronal heating [14], and one that is compatible with the perpendicular cascade. In contrast, direct cyclotron absorption appears to require a strong parallel cascade [97], which is difficult to justify based on MHD turbulence theory (see e.g., [34]). In any case, the wealth of possible kinetic activity within and near turbulent driven small-scale reconnection sites should provide ample opportunity for conversion of MHD energy into heat.

We foresee that there is a wide scope of future possibilities to extend, generalize, and improve the current generation of turbulence models for heating the corona. In the evolution towards more realism, prominent improvements would be better boundary conditions, better models for transport effects, and improved models of the background coronal fields themselves. Ultimately, of course, the large-scale coronal fields, and even the accelerated solar wind, should be included dynamically in such models. At that point the entire framework would require generalization, and a self-consistent model would emerge. While turbulence and cascade of MHD-scale fluctuations will remain a feature of a self-consistent coronal heating formalism, it remains to be seen how far in the evolution of these models the convenient and compact RMHD approximation will carry us.

Appendix A: Alternative Derivations of RMHD

The original derivation of the RMHD equations was presented by Strauss [24], motivated by geometries and plasma conditions typical of fusion devices (e.g., low β_{p}, large aspect ratio tokamaks, significant nonlinearity). The treatment was perturbative with the small expansion parameter being the aspect ratio

$\epsilon_{\mathrm{Strauss}} = \ell_\perp/\ell_\parallel$, where the ℓ's characterise typical lengthscales perpendicular and parallel to the mean magnetic field, $\boldsymbol{B}_0$. Ordering the fully 3D variables and equations in $\epsilon_{\mathrm{Strauss}}$ and then dropping (i) all toroidal effects, and (ii) all terms of the same order as the toroidal ones, yields the RMHD equations.[18]

Subsequently, Montgomery [25] rederived the RMHD equations from a different perspective, based on the assumption of incompressible fluctuations, which although weak in amplitude (relative to a strong $\boldsymbol{B}_0$), were still strongly nonlinear. In this case the small expansion parameter is expressible as $\epsilon_{\mathrm{Mont}} = \delta b/B_0$, where δb is the RMS magnetic fluctuation. This derivation also retained the viscous and resistive dissipation terms, and included discussion of the distinctive nature of spectral transfer in RMHD (see also [32]).

The conditions under which low Mach number compressible 3D MHD systems can be described using the equations of 2D or 3D incompressible MHD, $2\frac{1}{2}$D incompressible MHD, or RMHD were carefully considered by Zank and Matthaeus [26], from both physical and rigorously mathematical standpoints. As a small parameter they employed the sonic Mach number, $\epsilon_{\mathrm{ZM}} \equiv M_{\mathrm{s}} = u_0/c_{\mathrm{s}}$, where u_0 is the RMS velocity and c_{s} is the sound speed. As they showed, RMHD is the appropriate leading-order description when the system is characterised by (i) a small aspect ratio, with an applied uniform magnetic field along the "long" dimension, (ii) either $\beta_{\mathrm{p}} \ll 1$ or $\beta_{\mathrm{p}} \approx 1$, and (iii) elimination of all high-frequency (i.e., acoustic timescale or faster) modes.

Starting from the fully 3D compressible MHD equations with $\beta_{\mathrm{p}} \leq 1$, Bhattacharjee et al. [40] have derived a "four-field" system of equations for situations where the mean field $\boldsymbol{B}_0$ is allowed to vary slowly. These equations reduce to those of RMHD in the case that $\boldsymbol{B}_0$ is uniform.

The derivation sketched in Sect. 2 is based on the requirement that the (global) nonlinear timescale is not slower than the wave timescale, and it is easy to see that this involves the ratio of the Strauss and Montgomery small parameters:

$$\frac{\tau_{\mathrm{NL}}}{\tau_{\mathrm{A}}} = \frac{\ell_\perp}{\delta b}\Big/\frac{\ell_\parallel}{B_0} = \frac{\ell_\perp}{\ell_\parallel}\frac{B_0}{\delta b} = \frac{\epsilon_{\mathrm{Strauss}}}{\epsilon_{\mathrm{Mont}}} \equiv \epsilon_{\mathrm{RMHD}} \lesssim 1. \tag{7}$$

As in the Zank and Matthaeus derivation, this approach emphasizes that it is the *timescales* of the fluctuations which determine whether or not RMHD is an appropriate approximation to use. In this sense these derivations unify those of Strauss and Montgomery.

Recently, several other derivations related to the RMHD equations have been given. Gazol et al. [99,100] showed that when the compressible MHD equations are perturbatively expanded using the *Alfvénic* Mach number as the small parameter, one also obtains equations related to the RMHD ones. Specifically, the transverse dynamics is governed by the usual RMHD equations while the parallel dynamics (with the same timescale) is governed by a generalized derivative nonlinear Schrödinger equation. In related simulation studies, Del Zanna et al.

---

[18] Strauss [24] notes that his motivation for deriving the RMHD equations was as a 3D generalisation of a (nonlinear) 2D approximation derived for tokamaks [98].

[101,102] have shown that the propagation of Alfvén waves in a 3D compressible medium can lead to the formation of perpendicular structures, which may be connected with RMHD dynamics. Similarly, Laveder et al. [103] showed that in a system governed by the Hall-MHD equations, driving with finite amplitude dispersive Alfvén waves can produce transverse dynamics governed by the RMHD equations. In such cases, RMHD dynamics coexists with the propagation of *small*-scale Alfvén waves, thereby providing an example of the broader validity of the RMHD description.

Note that *none of these derivations of RMHD are linearizations* of the MHD equations: in RMHD the nonlinearities are always important (by construction). Indeed, there is no linearized version of RMHD, since the nonlinear terms cannot become small relative to the the linear (wave propagation) terms without violating the timescale assumptions used to derive the RMHD equations. RMHD fluctuations are intrinsically nonlinear.[19] Nonetheless, as discussed in Appendix B, the non-RMHD modes, which contain the linear wave solutions of the incompressible MHD equations, can still be simulated within the RMHD equations.

Finally, we note that the "critical balance" condition employed in a consideration of the energy spectra in strong incompressible MHD turbulence [29] is equivalent to the modal RMHD condition $\epsilon_{\mathrm{RMHD}}(\boldsymbol{k}) \lesssim 1$, in the sense that critical balance, defined as $\tau_{\mathrm{NL}} = \tau_{\mathrm{A}}$, describes the RMHD boundary (cf. Fig. 7a).

Appendix B: Self-Consistency of RMHD Simulations

To obtain the k-space boundary curve which (roughly) separates the RMHD and non-RMHD fluctuations it is necessary to know the functional forms for the dependence of the energy spectrum on $k_\perp$ and k_z. For example, assuming a powerlaw perpendicular spectrum $\sim k_\perp^{-\alpha}$, and an approximately flat parallel spectrum, the modal RMHD condition, $\tau_{\mathrm{NL}}(\boldsymbol{k}) \lesssim \tau_{\mathrm{A}}(\boldsymbol{k})$, becomes $k_\perp \propto k_z^{2/(3-\alpha)}$. For the $\alpha = 5/3$ Kolmogorov case this becomes $k_\perp \propto k_z^{3/2}$. Such a curve is sketched in Figure 7a. Note that this description of the limits of applicability of RMHD can be no more that an approximation in general, since turbulence may not be driven or steady, as would be required to attain a strict (inertial range) powerlaw; also, the dependence of the spectrum upon k_z is likely to be more complicated than that assumed above.

An interesting point then arises in connection with simulations employing the RMHD equations. Since these equations are valid for RMHD fluctuations, they should not, strictly speaking, be used to evolve non-RMHD modes. However, as Fourier-space simulation domains are often rectangular in shape, the set of excited fluctuations is likely to include both RMHD and non-RMHD modes, as indicated in Figure 7a. One is then led to consider the self-consistency of such simulations, and in particular whether or not non-RMHD modes behave in an (essentially) correct fashion when simulated via the RMHD equations.

---

[19] The exception to this is the subset of RMHD modes which are actually 2D (i.e., they have $k_\parallel = 0$). Hence, for these modes there is no parallel-propagation timescale with which to compare their nonlinear timescale.

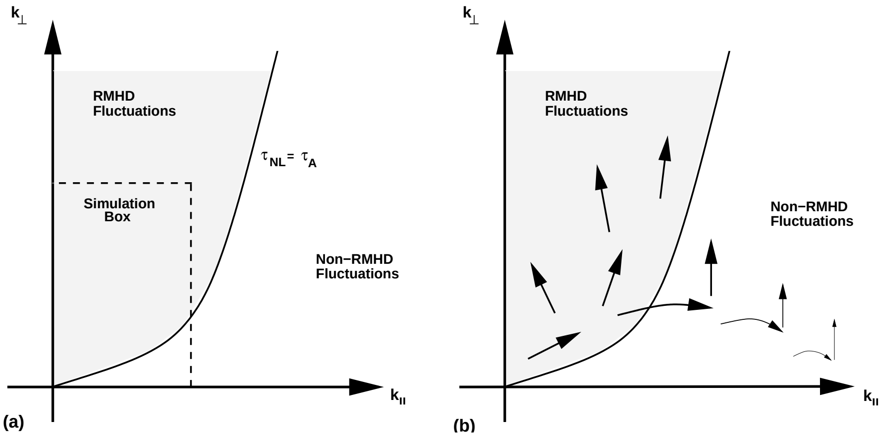

Fig. 7. (a) Cartoon sketch of the (spectral) boundary between the RMHD modes and the non-RMHD modes. The system is assumed to be in approximate steady-state, with an energy spectrum which is Kolmogorov-like in the perpendicular direction and approximately flat in the parallel direction. A typical simulation domain (*dotted*) is also indicated. **(b)** Indications of the direction and strength of spectral transfer for RMHD and non-RMHD modes. The width of the arrows suggests the strength of the transfer

In the case of periodic boundary conditions it appears that the situation is indeed self-consistent. Figure 8 shows results from forced[20] RMHD simulations at resolution $64^2 \times 32$ and Reynolds numbers of 200. Shown are the steady parallel energy spectra $E_z(k_z) = \int E(k_x, k_y, k_z)\, \mathrm{d}k_x \mathrm{d}k_y$, as a function of k_z, for five values of B_0 ranging from 1/2 to 8. The simulations from which the plots are made all start with identical initial data and Reynolds numbers, with only the value of B_0 different in each run. Note that the values of B_0 are all large, since the physical mean field is given by B_0/ϵ (see Sect. 2.1), where ϵ is considered to have the same fixed value in each simulation.

The solid curve is for the "standard" RMHD situation of $B_0 = 1$. Clearly, larger values of B_0 lead to spectra which are significantly steeper and therefore associated with weaker parallel cascades. There is even some suggestion of a range where the falloff is exponential, especially for the larger values of B_0.[21]

Our interpretation of this result is that the essential physics for the non-RMHD modes is still retained in the RMHD equations. More specifically, counter-propagating Alfvénic wavepackets will only overlap for a time $t \approx \lambda_{\|}/(2V_A)$, where $\lambda_{\|}$ is a parallel lengthscale characteristic of the packets. If this time is *shorter* than the corresponding τ_{NL} then the interaction generates destructive interference rather than a spectral cascade.

---

[20] The forcing consists of driving a unidirectional Alfvén wave with a $\boldsymbol{k} = (1, 1, 1)$.

[21] The increases at the highest values of k_z appear to be real properties of the numerical approximation and we suspect they are associated with energy "splashing" at the max k_z "walls", since there is no dissipation in this direction.

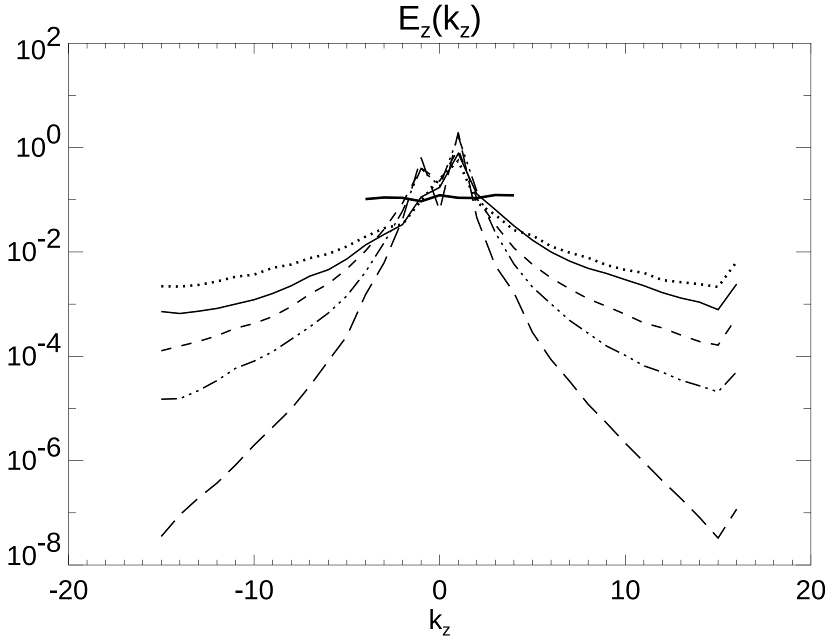

Fig. 8. Steady parallel energy spectra $E_z(k_z)$ for forced $64^2 \times 32$ RMHD simulations with various values of B_0. From top to bottom the values of B_0 are 1/2 (*dots*), 1, 2, 4, and 8 (*long dashes*). Note the steeper spectra for larger B_0, indicating a weakened parallel cascade. The heavy (roughly) horizontal line is the initial condition

We close with a physical argument as to why the parallel spectrum could be exponential in k_z.[22] In the interaction of two Fourier modes, most of the excitation will be transferred to higher $\boldsymbol{k}_\perp$, at nearly fixed k_z (see Fig. 7b). However, some excitation will undergo parallel spectral transfer to a new k_z. The process then repeats at this (typically larger) k_z and such a survivalist process could easily produce an exponential spectrum in k_z. A fuller discussion of the topic of this appendix is being prepared for publication.

Acknowledgments

Special thanks to Peter Ulmschneider, for his kind permission to include Table 1, and to Marco Velli, for insightful conversations regarding RMHD and coronal physics. We also acknowledge many useful and instructive conversations with David Montgomery, who suggested the exponential parallel RMHD spectrum nearly twenty years ago. This work has been supported by grants from the UK PPARC (PPA/G/S/1999/00059), NASA, and the NSF.

---

[22] The first clear statement that the parallel spectrum should be exponential while the perpendicular spectrum should be $k^{-5/3}$ for MHD in a strong external magnetic field appears to be due to Montgomery [104, p. 139].

References

1. W. Grotrian: Naturwissen **27**, 214 (1939)
2. B. Edlén: Z. Astrophys. **22**, 30 (1942)
3. U. Narain, P. Ulmschneider: Space Sci. Rev. **54**, 377 (1990)
4. U. Narain, P. Ulmschneider: Space Sci. Rev. **75**, 453 (1996)
5. P. Ulmschneider: 'Alfvén wave propagation in the solar corona and inner heliosphere'. In: *Cool Stars, Stellar Systems and the Sun*, ed. by R. Pallavicini, A.K. Dupree (PASP Conf. Series Vol 109, 1996)
6. P. Ulmschneider, E.R. Priest, R. Rosner: *Mechanisms of Chromospheric and Coronal Heating* (Springer, Berlin, 1991)
7. L. Golub, J.M. Pasachoff: *The Solar Corona* (CUP, Cambridge, 1997)
8. M. Velli: 'Coronal heating, nanoflares and MHD turbulence'. In: *Solar Wind Eight*, ed. by D. Winterhalter, J.T. Gosling, S.R. Habbal, W.S. Kurth, M. Neugebauer (AIP, New York, 1996), p. 28
9. J.L. Kohl et al.: Space Sci. Rev. **72**, 29 (1995)
10. J.L. Kohl et al.: Solar Phys. **175**, 613 (1997)
11. J. Chae, U. Schühle, P. Lemaire: Astrophys. J. **505**, 957 (1998)
12. R.R. Grall, W.A. Coles, M.T. Klinglesmith, A.R. Breen, P.J.S. Williams, J. Markkanen, R. Esser: Nature **379**, 429 (1996)
13. S.R. Cranmer, G.B. Field, J.L. Kohl: Astrophys. J. **518**, 937 (1999)
14. W.I. Axford, J.F. McKenzie: 'The solar wind'. In: *Cosmic Winds and the Heliosphere* (Arizona U. Press, 1997), p. 31
15. J.L. Culhane: Adv. Space Res. **19**, 1839 (1998)
16. F. Califano, C. Chiuderi: Physica Scripta **T75**, 197 (1998)
17. F. Califano, C. Chiuderi: Phys. Rev. E **60**, 4701 (1999)
18. A. Barnes: 'Hydromagnetic waves and turbulence in the solar wind'. In: *Solar System Plasma Physics, vol. I*, ed. by E.N. Parker, C.F. Kennel, L.J. Lanzerotti (North-Holland, Amsterdam, 1979), p. 251
19. A. Mangeney, R. Grappin, M. Velli: 'MHD turbulence in the solar wind'. In: *Advances in Solar System Magnetohydrodynamics*, ed. by E.R. Priest, A.W. Hood (CUP, Cambridge, 1991), p. 327
20. C.Y. Tu, E. Marsch: Space Sci. Rev. **73**, 1 (1995)
21. W.H. Matthaeus, J.W. Bieber, G.P. Zank: Rev. Geophys. Supp. **33**, 609 (1995)
22. J.C. Vial, B. Kaldeich-Schürmann, eds.: *Proc. of the 8th SoHO Workshop 'Plasma Dynamics and Diagnostics in the Solar Transition Region and Corona'*, vol. ESA SP-446 (ESA, Noordwijk, The Netherlands, 1999)
23. S. Masuda, T. Kosugi, H. Hara, S. Tsuneta, Y. Ogawara: Nature **371**, 495 (1994)
24. H.R. Strauss: Phys. Fluids **19**, 134 (1976)
25. D.C. Montgomery: Physica Scripta **T2/1**, 83 (1982)
26. G.P. Zank, W.H. Matthaeus: J. Plasma Phys. **48**, 85 (1992)
27. W.H. Matthaeus, S. Ghosh, S. Oughton, D.A. Roberts: J. Geophys. Res. **101**, 7619 (1996)
28. G.K. Batchelor: *The Theory of Homogeneous Turbulence* (CUP, Cambridge, 1970)
29. P. Goldreich, S. Sridhar: Astrophys. J. **438**, 763 (1995)
30. R. Kinney, J.C. McWilliams: Phys. Rev. E **57**, 7111 (1998)
31. S. Oughton, S. Ghosh, W.H. Matthaeus: Phys. Plasmas **5**, 4235 (1998)
32. D.C. Montgomery, L. Turner: Phys. Fluids **24**, 825 (1981)
33. J.V. Shebalin, W.H. Matthaeus, D. Montgomery: J. Plasma Phys. **29**, 525 (1983)

34. R.L. Leamon, W.H. Matthaeus, C.W. Smith, G.P. Zank, D.J. Mullan, S. Oughton: Astrophys. J. **537**, 1054 (2000)
35. R. Grappin: Phys. Fluids **29**, 2433 (1986)
36. S. Galtier, S.V. Nazarenko, A.C. Newell: Nonlin. Process. Geophys. **8**, 1 (2001)
37. V. Carbone, P. Veltri: Geophys. & Astrophys. Fluid Dynam. **52**, 153 (1990)
38. S. Oughton, E.R. Priest, W.H. Matthaeus: J. Fluid Mech. **280**, 95 (1994)
39. W.H. Matthaeus, S. Oughton, S. Ghosh, M. Hossain: Phys. Rev. Lett. **81**, 2056 (1998)
40. A. Bhattacharjee, C.S. Ng, S.R. Spangler: Astrophys. J. **494**, 409 (1998)
41. J. Cho, E.T. Vishniac: Astrophys. J. **539**, 273 (2000)
42. S. Galtier, S.V. Nazarenko, A.C. Newell, A. Pouquet: J. Plasma Phys. **63**, 447 (2000)
43. C.S. Ng, A. Bhattacharjee: Astrophys. J. **465**, 845 (1996)
44. J.G. Doyle, E. OShea, R. Erdelyi, K.P. Dere, D.G. Socker, F.P. Keenan: Solar Phys. **173**, 243 (1997)
45. Y.Q. Hu, R. Esser, S.R. Habbal: J. Geophys. Res. **102**, 14661 (1997)
46. H.P. Warren, J.T. Mariska, K. Wilhelm, P. Lemaire: Astrophys. J. **484**, L91 (1997)
47. G. Einaudi, M. Velli, H. Politano, A. Pouquet: Astrophys. J. **457**, L113 (1996)
48. W.H. Matthaeus, G.P. Zank, S. Oughton: 'Coronal heating by quasi-2D MHD turbulence driven by non-WKB wave reflection'. In: *Solar Wind Nine*, ed. by S. Habbal, R. Esser, J.V. Hollweg, P.A. Isenberg (AIP, Woodbury, NY, 1999), vol. 471, pp. 361–364
49. W.H. Matthaeus, G.P. Zank, S. Oughton, D.J. Mullan, P. Dmitruk: Astrophys. J. **523**, L93 (1999)
50. S. Oughton, W.H. Matthaeus, G.P. Zank, D.J. Mullan: 'Coronal heating via Alfvén waves and 2D MHD turbulence'. In: *Proc. of the 8th SoHO Workshop 'Plasma Dynamics and Diagnostics in the Solar Transition Region and Corona'*, ed. by J.C. Vial, B. Kaldeich-Schürmann (ESA, Noordwijk, The Netherlands, 1999), vol. ESA SP-446, pp. 525–530
51. S. Oughton, W.H. Matthaeus, P. Dmitruk, L.M. Milano, G.P. Zank, D.J. Mullan: Astrophys. J. **551**, 565 (2001)
52. P. Dmitruk, W.H. Matthaeus, L.J. Milano, S. Oughton: Phys. Plasmas **8**, 2377 (2001)
53. P. Dmitruk, L.J. Milano, W.H. Matthaeus: Astrophys. J. **548**, 482 (2001)
54. E.N. Parker: Astrophys. J. **372**, 719 (1991)
55. J. McKenzie, M. Banaszkiewicz, W.I. Axford: Astron. Astrophys. **303**, L45 (1995)
56. C.Y. Tu, E. Marsch: Solar Phys. **171**, 363 (1997)
57. S.R. Spangler, S. Mancuso: Astrophys. J. **530**, 491 (2000)
58. R.L. Moore, Z.E. Musielak, S.T. Suess, C.H. An: Astrophys. J. **378**, 347 (1991)
59. Z.E. Musielak, J.M. Fontenia, R.L. Moore: Phys. Fluids B **4**, 13 (1992)
60. Y. Zhou, W.H. Matthaeus: J. Geophys. Res. **95**, 14 863 (1990)
61. M. Velli: Astron. Astrophys. **270**, 304 (1993)
62. M. Dobrowolny, A. Mangeney, P. Veltri: Phys. Rev. Lett. **45**, 144 (1980)
63. W.H. Matthaeus, D. Montgomery: 'Dynamic alignment and selective decay in MHD '. In: *Statistical Physics and Chaos in Fusion Plasmas*, ed. by C.W.J. Horton, L.E. Reichl (Wiley, New York, 1984), p. 285
64. G. Einaudi, M. Velli: Phys. Plasmas **6**, 4146 (1999)
65. P. Dmitruk, D.O. Gómez: Astrophys. J. **484**, L83 (1997)
66. J.V. Hollweg: Solar Phys. **70**, 25 (1981)

67. Y. Zhou, W.H. Matthaeus: J. Geophys. Res. **95**, 10 291 (1990)
68. J. Maron, P. Goldreich: Astrophys. J. **554**, 1175 (2001)
69. R.H. Kraichnan: Phys. Fluids **8**, 1385 (1965)
70. R. Grappin, U. Frisch, J. Léorat, A. Pouquet: Astron. Astrophys. **105**, 6 (1982)
71. A. Pouquet, U. Frisch, M. Meneguzzi: Phys. Rev. A **33**, 4266 (1986)
72. S. Ghosh, W.H. Matthaeus, D. Montgomery: Phys. Fluids **31**, 2171 (1988)
73. E.N. Parker: Astrophys. J. **174**, 499 (1972)
74. E.N. Parker: Astrophys. J. **264**, 642 (1983)
75. E.N. Parker: Astrophys. J. **330**, 474 (1988)
76. A.A. van Ballegooijen: Astrophys. J. **311**, 1001 (1986)
77. N.F. Otani, H.R. Strauss: Astrophys. J. **325**, 468 (1988)
78. H.R. Strauss, N.F. Otani: Astrophys. J. **326**, 418 (1988)
79. D.O. Gómez, C. Ferro Fontán: Solar Phys. **116**, 33 (1988)
80. D.O. Gómez, C. Ferro Fontán: Astrophys. J. **394**, 662 (1992)
81. Z. Mikić, D.C. Barnes, D.D. Schnack: Astrophys. J. **328**, 830 (1988)
82. Z. Mikić, D.D. Schnack, G. Van Hoven: Astrophys. J. **338**, 1148 (1989)
83. J. Heyvaerts, E.R. Priest: Astrophys. J. **390**, 297 (1992)
84. D.W. Longcope, R.N. Sudan: Astrophys. J. **384**, 305 (1992)
85. D.W. Longcope, R.N. Sudan: Astrophys. J. **437**, 491 (1994)
86. D.W. Longcope, H.R. Strauss: Astrophys. J. **426**, 742 (1994)
87. D.L. Hendrix, G. van Hoven: Astrophys. J. **467**, 887 (1996)
88. P. Dmitruk, D.O. Gómez, E.E. DeLuca: Astrophys. J. **505**, 974 (1998)
89. P. Dmitruk, D.O. Gómez: Astrophys. J. **527**, L63 (1999)
90. C.H. Mandrini, P. Demoulin, J.A. Klimchuk: Astrophys. J. **530**, 999 (2000)
91. D.O. Gómez, P. Dmitruk, L.J. Milano: Solar Phys. **195**, 299 (2000)
92. T.E. Berger, A.M. Title: Astrophys. J. **463**, 365 (1996)
93. D.M. Hassler, G.J. Rottman, E.C. Shoub, T.E. Holzer: Astrophys. J. **348**, L77 (1990)
94. W.H. Matthaeus, S.L. Lamkin: Phys. Fluids **29**, 2513 (1986)
95. M.A. Shay, J.F. Drake, R.E. Denton, D. Biskamp: J. Geophys. Res. **103**, 9165 (1998)
96. R.E. Ergun, C.W. Carlson, J.P. McFadden, F.S. Mozer, L. Muschietti, R. I., R.J. Strangeway: Phys. Rev. Lett. **81**, 826 (1998)
97. S.R. Cranmer: Astrophys. J. **532**, 1197 (2000)
98. M.N. Rosenbluth, D.A. Monticello, H.R. Strauss, R.B. White: Phys. Fluids **19**, 1987 (1976)
99. A. Gazol, T. Passot, P.L. Sulem: Phys. Plasmas **6**, 3114 (1999)
100. A. Gazol, T. Passot, P.L. Sulem: Rev. Mex. A. A. **9**, 80 (2000)
101. L. Del Zanna: Geophys. Rev. Lett. **28**, 2585 (2001)
102. L. Del Zanna, M. Velli, P. Londrillo: Astron. Astrophys. **367**, 705 (2001)
103. D. Laveder, T. Passot, P.L. Sulem: Phys. Plasmas **9**, 305 (2002)
104. D.C. Montgomery: *Lecture Notes on Turbulence* (World Scientific, Singapore, 1989), p. 75. Lecture Notes from the NCAR-GTP Summer School, June 1987